remote sensing

Article

Pointwise Modelling and Prediction for Ground Surface Uplifts in Abandoned Coal Mines from InSAR Observations

Xiwen Yin [1], Jiayao Chai [2], Weinan Deng [1,3], Zefa Yang [2,*], Guochan Tian [1,3] and Chao Gao [1,3]

1 Coal Mining Research Institute, China Coal Technology and Engineering Group, Beijing 100013, China
2 School of Geosciences and Info-Physics, Central South University, Changsha 410083, China
3 Tiandi Science & Technology Co., Ltd., Beijing 100013, China
* Correspondence: yangzf@csu.edu.cn

Abstract: Interferometric synthetic aperture radar (InSAR) is a useful tool for monitoring surface uplifts due to groundwater rebound in abandoned coal mines. However, InSAR-based prediction for surface uplifts has rarely been focused on so far, hindering the scientifical assessment and controlling of uplift-related geohazards in a wide area. In this study, we firstly revealed that the temporal evolution of surface uplifts caused by groundwater rebound at a surface point approximately followed an exponential distribution. Following the result, a varied cumulative distribution function (CDF) of the Weibull distribution was then used to model the temporal evolution of surface uplifts on a point-by-point basis. Finally, the parameters of the varied Weibull CDF were inverted from historical InSAR observations of surface uplifts and were forward used to predict uplift trends. Two abandoned coal mines in Beipiao city, China, were chosen to test the presented method. The results suggest that the varied Weibull CDF is able to well describe the processing of time-series uplifts, and the root mean square errors of the predicted uplifts were about 1.2 mm. The presented pointwise method predicts surface uplifts based on historical uplift observations and a mathematical function (i.e., the varied Weibull CDF), without the requirement of in situ geological and hydrological information about the focused abandoned coal mines. Therefore, it offers a new tool for predicting surface uplifts in abandoned mines, especially in case they lack in situ geological and hydrological information.

Keywords: abandoned coal mines; InSAR; exponential distribution; Weibull distribution; surface uplifts

check for updates

Citation: Yin, X.; Chai, J.; Deng, W.; Yang, Z.; Tian, G.; Gao, C. Pointwise Modelling and Prediction for Ground Surface Uplifts in Abandoned Coal Mines from InSAR Observations. *Remote Sens.* **2023**, *15*, 2337. https://doi.org/10.3390/rs15092337

Academic Editors: Yiping Wu, Török Ákos, Fasheng Miao and Abdolreza Ghods

Received: 22 February 2023
Revised: 25 April 2023
Accepted: 25 April 2023
Published: 28 April 2023

1. Introduction

The changes of the energy market and the increasing concern for global climate changes have led to the closure of many deep coal mines worldwide [1,2]. After the closure of a deep coal mine, the pumping of groundwater is generally halted. As a consequence, surface water and/or overlying aquifer water may flood into the mined voids and surrounding strata trough channels, such as fractures and faults, resulting in groundwater rebound. Groundwater rebound in abandoned mines can cause ground surface uplift, imposing damage threats on infrastructures (e.g., buildings, railway, pipes, communication or electric towers, and so forth) [3]. Therefore, it is important to accurately monitor and forward predict surface uplifts induced by groundwater rebound in abandoned coal mines.

Interferometric synthetic aperture radar (InSAR) is able to monitor ground surface displacements in a wide area with high spatial resolution and low cost. In recent decades, numerous time-series InSAR algorithms, such as the Stanford method for persistent scatterers [4], SqueeSAR [5], and small baseline subset InSAR (SBAS-InSAR) [6], have been proposed to detect ground surface time-series displacements. Readers can refer to [7,8] for a review on time-series InSAR techniques. InSAR is a promising tool to detect surface displacements induced by natural landslide, earthquake and underground mining activities, and so forth [9–19]. Owing to the distinctive advantages of InSAR, in 2013, InSAR was applied to monitor surface uplift in the abandoned coal mines in Limburg, Netherlands, for the first time [20]. Following that, InSAR has been widely used to detect historical surface uplift in numerous abandoned mines in China, Germany, Poland, the United Kingdom, and so forth [21–26]. Readers can refer to Zhao and Konietzky [27] for a review on this topic.

In fact, surface uplift monitoring in abandoned mines using InSAR is well-developed and state-of-the-art. However, only a few studies have focused on surface uplift prediction from InSAR observations. In 2020, Zhao and Konietzky [28] proposed an approach for predicting groundwater rebound-induced surface uplift in abandoned mines with elasto-plastic numerical modeling and InSAR uplift observations. The numerical approach is theoretically able to consider the physical coupling behaviors of complex geological and hydrological situations in abandoned mines. Since detailed information on mining situations, geology, and hydrology are required by the numerical approach, it is difficult to reliably predict surface uplift if the required information is lack or insufficient. In the same year, Gee et al. [11] proposed an analytical approach to predict surface uplift by incorporating InSAR observations with the principle of effective stress. Compared with the numerical approach proposed by Zhao and Konietzky, the analytical approach requires less information about geology and hydrology. In this regard, the analytical approach can be used in a wide area with relatively simple calculations [26]. Even so, some geological and hydrological parameters (e.g., geostatic pressure, void ratio, and coefficient of volume compressibility) and groundwater levels are still needed. This, to a large extent, limits the practical applications of the analytical approach, especially over those abandoned mines where the needed parameters are lacking.

To circumvent this, we proposed an empirical approach to predict surface uplift in abandoned mines from InSAR uplift observations. Firstly, an exponential function was selected to model the temporal evolution of surface uplift at a single point in abandoned mines. The parameters of the selected exponential function were then inverted based on InSAR observations of a historical time-series surface uplift. Thirdly, future surface uplift was predicted with the inverted parameters and the exponential function. Compared to the existing InSAR-based numerical and analytical approaches, the proposed mathematical approach in this study relied on InSAR observations alone. Therefore, it is able to work well in a wide area without the requirement of geological and hydrological field parameters.

2. Methods

2.1. Pointwise Modelling for Surface Uplifts with a Varied Weibull Distribution Function

Following the cessation of groundwater pumping in abandoned mines, the rising curve of groundwater levels approximately follows an exponential distribution [20,29–31]. Previous studies have suggested that there is a linearly positive correlation between groundwater level and surface uplift in abandoned mines [20,32]. Consequently, surface uplift induced by groundwater rebound at a single surface point can be assumed to follow an exponential distribution. The cumulative distribution function of an exponential distribution F_{exp} is given by the following:

$$F_{\text{exp}}(t, \lambda) = 1 - e^{-\lambda t} \quad t \geq 0 \tag{1}$$

where t denotes time; λ is the parameter of distribution (generally referred to as rate parameter).

Equation (1) is a single-parameter function, which may not describe well enough the temporal evolution of time-series uplift at a single surface point. Equation (2) shows the cumulative distribution function (CDF) of a two-parameter Weibull distribution,

$$F_{wei}(t, \eta, \beta) = 1 - e^{-(t/\eta)^{\beta}} \quad t \geq 0 \tag{2}$$

where η and β are the scale parameter and shape parameter, respectively. As is observed from Equation(2), the exponential distribution is a special case of the Weibull distribution (i.e., $\beta = 1$). Therefore, the Weibull distribution is more flexible for describing surface time-series uplift in abandoned mines compared to exponential distribution.

However, it is noted that the maximum value of the Weibull CDF is one, which does not meet real scenarios in which the maximum surface uplift is varied in different abandoned mines. To circumvent this, a parameter for describing the varied maximum surface uplift should be included in Equation (2), and surface time-series uplift caused by groundwater rebound at a single point (namely $d_u(t)$) can be described as a varied Weibull CDF, as follows:

$$d_u(t,P) = d_u^0 \cdot F_{wei}(t,\eta,\beta) = d_u^0\left[1 - e^{-(t/\eta)^\beta}\right], \quad t \geq 0 \tag{3}$$

where $P = \begin{bmatrix} d_u^0 & \eta & \beta \end{bmatrix}$ is the parameter matrix of the varied Weibull CDF, with d_u^0 being the maximum uplift parameter.

It should be noted that a probabilistic approach for InSAR time-series postprocessing was proposed in 2016 to model time-series InSAR observations [33]. In this approach, an optimal function was selected from a function library to describe the kinematic evolution of surface InSAR-measured displacements using multiple hypotheses testing. This approach models surface displacements in a mathematical view, without taking the physical processing of displacement events into account. The varied Weibull CDF is derived with the consideration of the physical processing of surface uplifts in abandoned coal mines; that is, the level change of groundwater rebound in abandoned coal mines follows an exponential distribution, and there is a linearly positive correlation between groundwater level and surface uplift. Therefore, this study offers a new view on modelling the kinematic evolution of surface displacements from InSAR observations.

2.2. Parameter Inversion of the Varied Weibull CDF

2.2.1. Retrieval of Surface Historical Uplift Using InSAR

In this section, the SBAS-InSAR algorithm is briefly reviewed. The SBAS-InSAR algorithm was first proposed by Berardino et al. [6] in 2002. Unlike the persistent scatterer InSAR (PS-InSAR) algorithm with an interferometric network of a single reference SAR image, SBAS-InSAR constructs an interferometric network with small-baseline multiple-reference SAR images by setting spatial and temporal baseline thresholds. Consequently, the influence of decorrelation due to long spatiotemporal baselines can be mitigated [34]. Owing to this merit, the SBAS-InSAR algorithm was selected to monitor surface uplifts in the following real data test.

The SBAS-InSAR algorithm is briefly reviewed below. Assuming that N co-registered SAR images acquired on the dates of $[t_0, t_1, \cdots, t_{N-1}]$ over the region of interest were firstly collected. M interferograms whose spatiotemporal baselines are both below a given threshold were then generated. Thirdly, the M interferograms were processed with the classical DInSAR procedure (e.g., topographic phase removal, filtering, phase unwrapping, and so forth) to generate M unwrapped phase maps. The phase at any point (x, y) in the i-th (i = 1,2, . . . ,M) unwrapped phase map is approximately represented as follows:

$$\Delta\varphi_i(x,y) = \varphi_{t_2} - \varphi_{t_1} = \frac{4\pi}{\lambda} d_{\mathrm{LOS}}(t_1,\ t_2) + \frac{4\pi}{\lambda} \cdot \frac{B_\perp}{R\sin\theta} \cdot \Delta z + \varphi_{resi} \tag{4}$$

where $\Delta\varphi_i$ is the i unwrapped phase; φ_{t_2} and φ_{t_1} are the phases at the acquisition dates t_1 and t_2; $B_\perp$ is the perpendicular baseline; R is the slant distance; θ is the incident angle; λ is the wavelength of SAR sensor; Δz and d_{LOS} denote height error and displacement, respectively; φ_{resi} is the residual phase, possibly including atmospheric delay and noise, etc.

Following the removal or mitigation of the residual phase and height error phase terms, displacements can be estimated based on Equation (4). More specifically, we firstly assume that the displacement in the time-adjacent acquisitions can be expressed as $d_{\mathrm{LOS}}(t_i,\ t_{i+1}) = v_i \cdot (t_i, -t_{i+1})$. Thus, the j-th unwrapped phase after the removal of residual phase and height error phase terms can be expressed by the accumulation of the time-adjacent displacement phases during the acquisition period of the j-th interferogram. Then, an equation system involving $N-1$ unknowns and M observation equations can be constructed. If $M \geq N$, ground surface displacement $d_{\text{LOS}}(t_i,\ t_{i+1})$ can be estimated by a least-square sense (over-conditioned) or singular-value decomposition (under-conditioned) algorithm.

Note that the displacements measured by InSAR techniques are along the line-of-sight (LOS) direction of the radar sensor, rather than the vertical direction (e.g., uplift in this study), due to the side-looking configuration of SAR sensors; that is, InSAR-measured LOS displacement (namely d_{LOS}) is the projection of the three-dimensional components of a real displacement vector in vertical, easting, and northing directions [35,36]:

$$d_{\text{LOS}} = d_u \cos\alpha + (d_{\text{n}} \sin\phi - d_{\text{e}} \sin\phi) \sin\alpha \tag{5}$$

where d_{u}, d_{n}, and d_{e} represent the three-dimensional displacement components in the vertical, northing, and easting directions, respectively; ϕ and α denote the flighting angle and incidence angle of the SAR sensor.

Equation (5) indicates that it is an ill-posed problem to accurately decompose the vertical component (i.e., subsidence or uplift) of a real displacement vector from single-track InSAR observations. Therefore, two options can be considered to estimate surface uplift in abandoned mines under the near-polar flighting configuration of the current InSAR satellites. The first one is assuming that only ground surface moves in the vertical direction only, and surface uplift can thus be estimated by:

$$d_{\text{u}} = d_{\text{LOS}} / \cos\alpha \tag{6}$$

When single-track InSAR observations are available for abandoned mines of interest. The second one is the fact that InSAR-measured LOS displacement is insensitive to the north displacement component under the near-polar flighting configuration of the current InSAR satellites. Consequently, under the assumption that the contribution of the north displacement component to LOS displacement is negligible, surface lift can thus be estimated by the following:

$$d_{\text{u}} = \frac{\sin\phi_{\text{des}} \cdot \cos\alpha_{\text{des}} \cdot (d_{\text{LOS}})_{\text{asc}} - \sin\phi_{\text{asc}} \cdot \cos\alpha_{\text{asc}} \cdot (d_{\text{LOS}})_{\text{des}}}{\sin\phi_{\text{des}} \cdot \cos\alpha_{\text{des}} \cdot \cos\alpha_{\text{asc}} - \sin\phi_{\text{asc}} \cdot \cos\alpha_{\text{asc}} \cdot \cos\alpha_{\text{des}}} \tag{7}$$

where InSAR-measured LOS displacements from ascending (denoted by the subscript of asc) and descending (denoted by the subscript of des) are both available for abandoned mines of interest.

2.2.2. Parameter Inversion with InSAR Observations of Surface Historical Uplifts

Having obtained the InSAR observations of surface historical uplift, the parameters of the two-parameter exponential distribution function can be inverted on a pixel-by-pixel basis. More specifically, Equation(3) is firstly transformed to be a linear function by a twice logarithmic operation, as follows:

$$y = \beta x - \varphi_0 \tag{8}$$

with $y = \log\left\{\log\left[\frac{1-d_u(t)}{d_u^0}\right]\right\}$, $x = \log t$, and $\varphi_0 = \beta \log \eta$. Let $t = \begin{bmatrix} t_1 & t_1 & \cdots & t_n \end{bmatrix}$ be the n dates of SAR acquisitions over the region of interest, and $d_u(t)$ be the time-series InSAR observations of historical uplift at a single surface point. The estimates of the parameters of the varied Weibull distribution (namely $\hat{P} = \begin{bmatrix} \hat{d}_u^0 & \hat{\eta} & \hat{\beta} \end{bmatrix}$) are finally estimated with a linear regression using Equation (8) on a pixel-by-pixel basis.

2.3. Prediction for Surface Uplift Using the Varied Weibull CDF

Having obtained the estimates of the varied Weibull distribution function at each highly coherent pixel in InSAR-measured uplift maps, future surface uplift can be predicted using Equation (3) on a pixel-by-pixel basis. The presented empirical method is capable of predicting surface uplift in abandoned mines based on InSAR observations and the varied Weibull distribution function only. Therefore, it is independent of geological and hydrological parameters relating to regions of interest, offering a new option to predict surface uplift induced by groundwater rebound in a wide area.

3. Study Area and SAR Data

3.1. Study Area

Two abandoned coal mines (i.e., Taiji and Guanshan) in Beipiao city (marked by a red circle in Figure 1a), China, were selected to test the presented InSAR-based empirical approach for predicting surface uplift. As is shown in Figure 1b, the Taiji coal mine is located in the south-west part of Beipiao city, and the normally mechanizing extraction there was started in the year of 1966, with a maximum mining depth over 800 m. The Guanshan coal mine is located in the north-east region of Beipiao city, whose normally mechanizing extraction was started in the 1950s at a maximum mining depth of 1059 m. The angles of the dip slope of coal seams in these two coal mines are about 35–67° to the horizontal direction, with a mean strike direction of around 78° from the north clockwise.

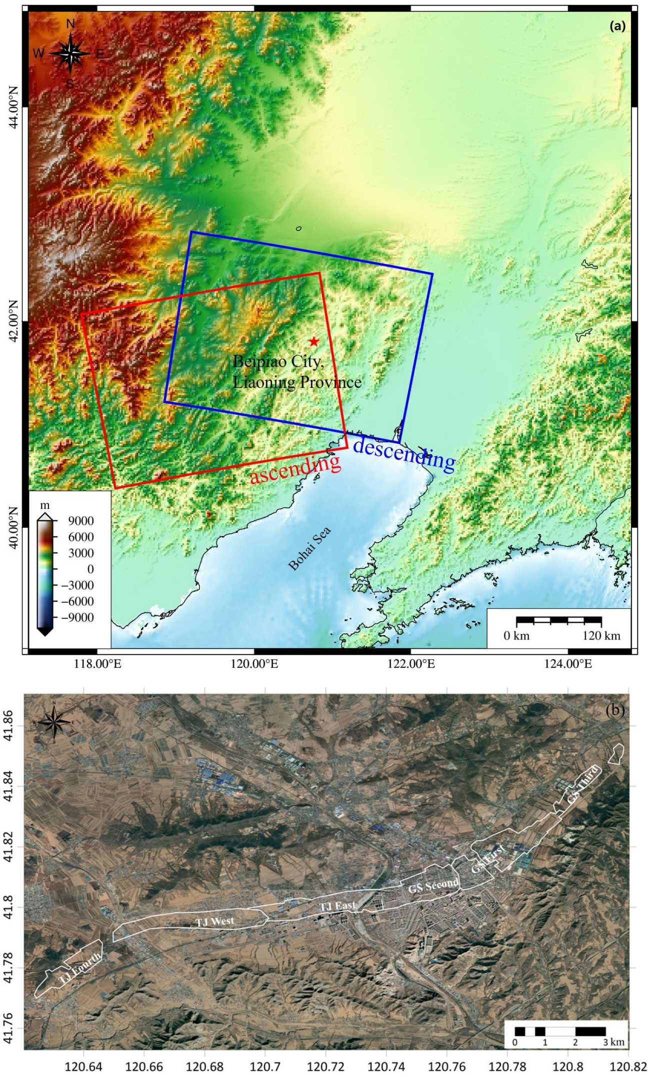

Figure 1. (**a**) Geological location of Beipiao city; (**b**) extraction regions of the Taiji (TJ) and Guanshan (GS) coal mines. The red and blue rectangles in (**a**) represent the footprints of the collected ascending and descending Sentinel-1 SAR images.

The focused Taiji and Guanshan coal mines were both closed in the year of 2014. Following the closure of the deep underground extraction, ground surface water and surface water and/or overlying aquifer water flooded into the mined-out voids and surrounding strata, causing ground surface uplift. The caused uplift imposes damage threats to surface buildings, roads, and other infrastructures in Beipiao city. Therefore, it is crucial to predict surface uplift induced by groundwater rebound there for assessing and controlling the potential damage threats.

3.2. SAR Data

To analyze the surface deformation status after the closure of the mining area in Beipiao City, this article used free and publicly available Sentinel-1 data and extracted the deformation information based on SBAS-InSAR technology. Sentinel-1 is an earth observation satellite developed by the European Space Agency. It is mainly equipped with C-band synthetic aperture radar. The system consists of two satellites, Sentinel-1A and Sentinel-1B (end of mission in August 2022 due to power issue). The repeated period of a single Sentinel-1 satellite is 12 days, which can be increased to 6 days with two Sentinel-1 satellites. In this study, 252 Sentinel-1A and 1B SAR images spanning from April 2017 to October 2021 over Beipiao city were collected. These SAR images were acquired by Sentinel-1 sensors in the Terrain Observation with Progressive Scans (TOPS) mode with ascending and descending orbits, respectively. The imaging parameters are shown in Table 1.

Table 1. Parameters of the collected Sentinel-1 SAR images.

Track	Observed Time	Number of Images	Heading	Incidence Angle
Ascending	4 April 2017–4 October 2021	130	−9.139	43.734
Descending	3 April 2017–3 October 2021	122	−169.886	39.184

4. Results

4.1. InSAR-Based Detection of Ground Surface Uplift

These collected ascending and descending Sentinel-1 SAR images were then processed with the SBAS-InSAR algorithm [6], in which a multi-look operation of 5:1 in the range and azimuth was firstly carried out in order to reduce interferometric noises. Secondly, a spatiotemporal baseline threshold of 150 m and 180 days was given, generating 257 and 241 small baseline interferograms from the ascending and descending Sentinel-1 SAR datasets. The spatiotemporal baseline networks of the generated small baseline interferograms are shown in Figure 2.

The generated small baseline interferograms were processed with a differential procedure, in which a non-local algorithm called block-matching and 3D filter for interferograms [37] was used to filter differential interferograms. The minimum cost flow algorithm [38] was chosen to unwrap phases. Then, high coherent pixels were selected with a minimum coherence of 0.3, and time-series LOS displacements were estimated using the classical processing of the SBAS-InSAR algorithm (e.g., linear displacement rate and height residual estimation, atmospheric delay mitigation, non-linear displacement component estimation). Having obtained time-series LOS displacements with the collected ascending and descending Sentinel-1 SAR acquisitions, respectively, surface uplifts in the two focused abandoned coal mines were finally estimated using Equation (7). The InSAR-measured rates and accumulative vertical displacements in the Taiji and Guanshan coal mines between April 2017 and October 2021 are shown in Figures 3 and 4, respectively.

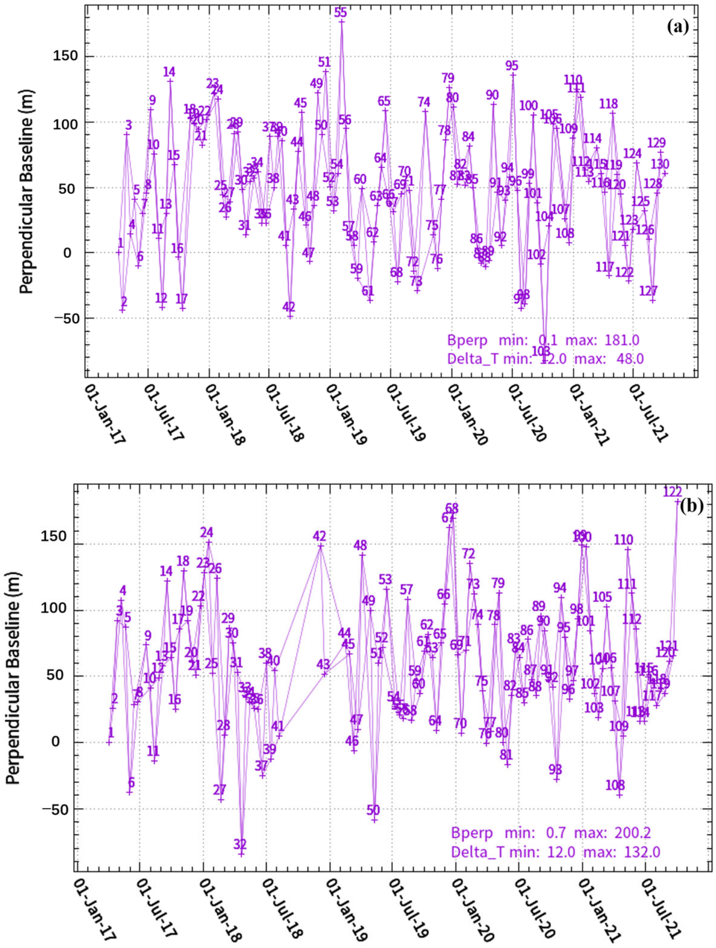

Figure 2. Spatiotemporal baseline networks for the generated ascending (**a**) and descending (**b**) small baseline interferograms.

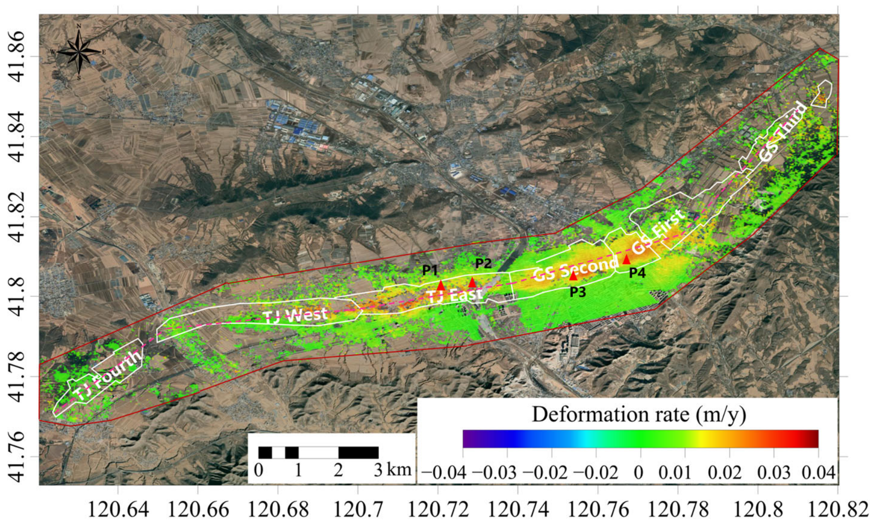

Figure 3. InSAR-measured rates of vertical displacements in the Taiji and Guanshan abandoned coal mines between April 2017 and November 2021. P1–P4 indicates four surface points with significant uplifts in the period of the collected SAR acquisitions.

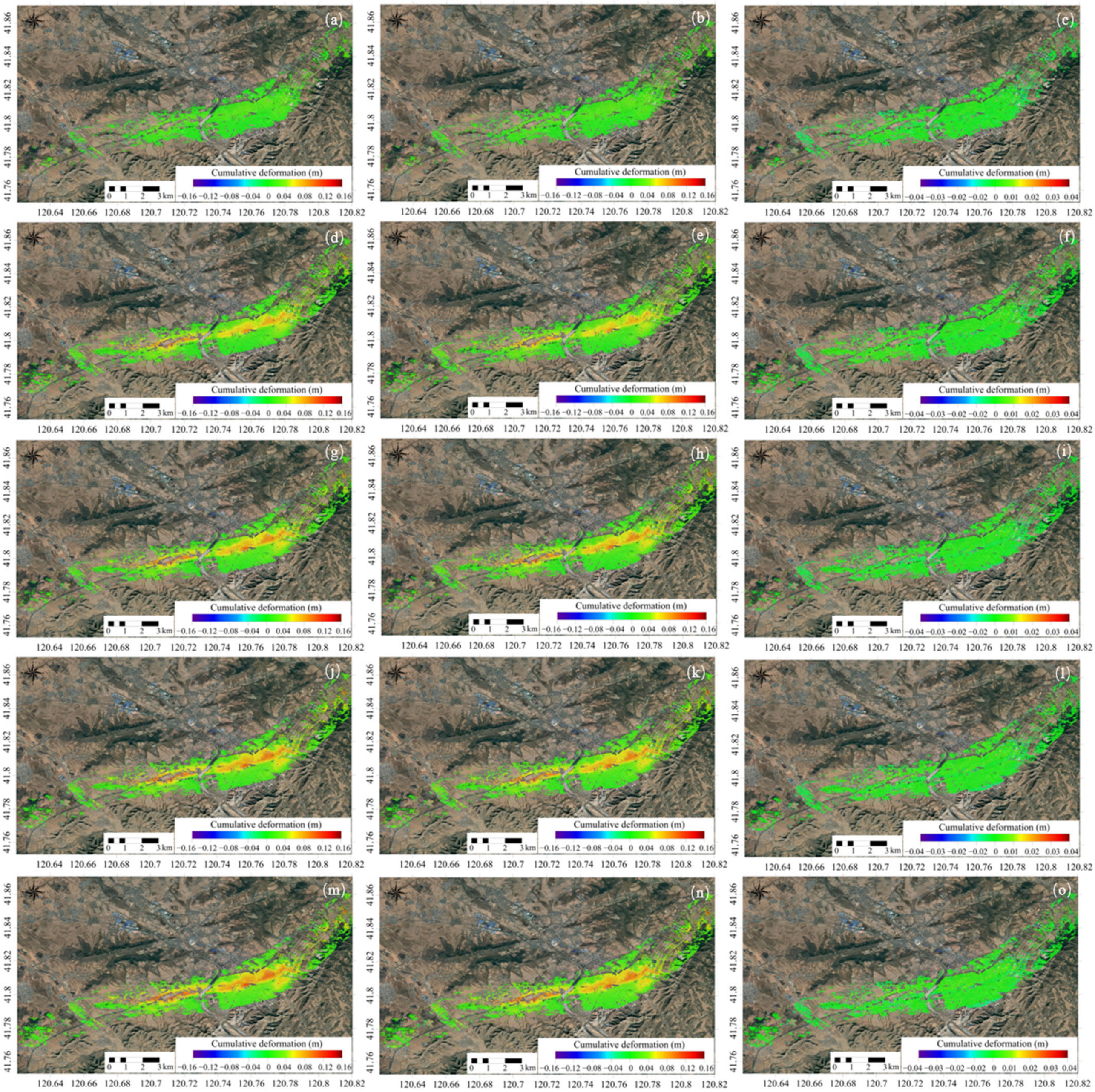

Figure 4. InSAR-measured (**a**,**d**,**g**,**j**,**m**) and Weibull-fitted (**b**,**e**,**h**,**k**,**n**) accumulative surface uplifts in the Taiji and Guanshan abandoned coal mines in December 2017, December 2018, December 2019, December 2020, and December 2021. (**c**,**f**,**i**,**l**,**o**) Residuals between the InSAR-measured and Weibull-fitted surface uplifts.

4.2. Pointwise Modelling for Surface Time-Series Uplifts

As is observed from Figure 4, the temporal evolution of time-series uplifts along the profile AA′ (marked by rose red dashed line in Figure 3) was non-linear. In this section, four surface points with significant uplifts in the period of the collected SAR acquisitions (named P1–P4 and marked by red triangles in Figure 3) were selected as samples to intuitively demonstrate the dynamic process of time-series uplift induced by groundwater rebound, in which the P1 and P2 points were situated in the Taiji abandoned coal mine, and the P3 and P4 points were located in the Guanshan coal mine. The InSAR-measured surface uplifts in these four points are shown in Figure 5.

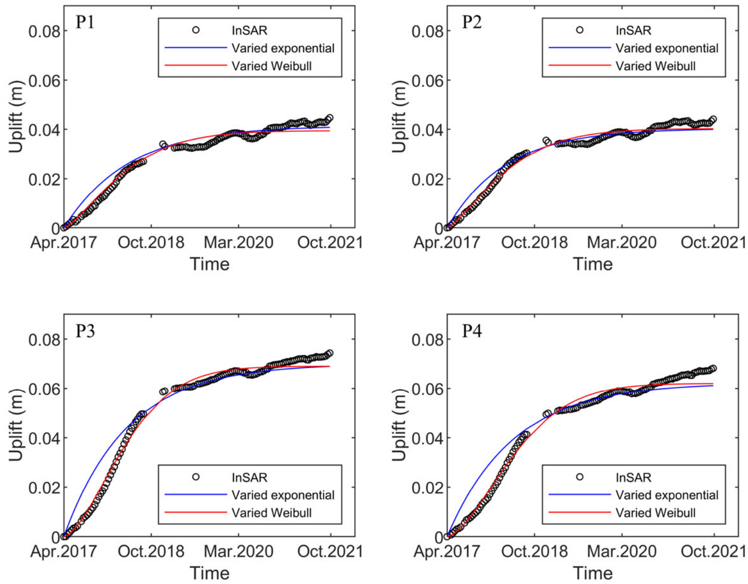

Figure 5. The performance comparison of fitting InSAR-measured surface uplift at point (**P1**–**P4**) (whose locations are marked by red triangles in Figure 3) with the varied exponential CDF and the varied Weibull CDF, respectively.

It can be seen from Figure 5 that the curve of time-series uplift at a single surface point approximately follows a CDF of exponential distribution; that is, ground surface uplifted exponentially increased following the closure of coal mines, and then the increasing rate was declined until zero (i.e., surface uplift remained stable). It was observed that the maximum uplifts of surface points in different locations were different; thus, the standard CDF of the exponential distribution (i.e., Equation (1) with a maximum of one) cannot describe the evolution processes of these four points well. This result proves that it is necessary to modify the CDF of the standard exponential distribution to be suitable to describe time-series surface uplifts caused by groundwater rebound at a single point.

To intuitively demonstrate the performance of the presented varied Weibull CDF on describing the temporal evolution of time-series uplift at a single surface point, we inverted the model parameters of the varied Weibull CDF based on Equation (8) using InSAR time-series uplifts at the four selected surface points, P1–P4. The time-series uplifts fitted by the varied Weibull CDF and its inverted model parameters at these four points are shown in Figure 5. R-squares, a widely-used indicator for evaluating the goodness of fit (the higher the better, and vice-versa), at these four points are listed in Table 2. As can be seen from Figure 5 and Table 2, the varied Weibull CDF can describe the temporal evolution of surface uplifts at a single point very well, with a mean R-square of about 0.99 for the four points. In addition, Akaike information criterion (AIC) scores, a measure for optimal model selection by weighting model performance and complexity (the lower the better, and vice-versa), are listed in Table 2. As is shown, the AIC scores of the varied Weibull CDF at these four points were much lower than the varied exponential function. This means that the varied Weibull CDF is better than the varied exponential function for describing the temporal evolution of surface uplifts in abandoned coal mines.

Table 2. Comparison of R-squares and AIC for fitting InSAR-measured surface uplift at points P1 to P4 with the varied exponential CDF and the varied Weibull CDF, respectively.

Point	R^2		AIC	
	Exponential	**Weibull**	**Exponential**	**Weibull**
P1	0.92	0.99	244	17
P2	0.93	0.99	161	58
P3	0.89	099	313	119
P4	0.74	0.98	323	61
Mean	0.87	0.99	260	64

Figure 6 plots the histograms of the residuals between the InSAR-measured and Weibull-fitted surface uplifts from December 2017 to December 2021 (Figure 6). It can be seen from Figure 6 that the residuals approximately followed normal distributions, with a mean of about zero and a standard deviation (STD) ranging from 0.8 mm to 1.7 mm. These results indicate that the varied CDF is able to describe the kinematic evolution of surface uplifts at a single point.

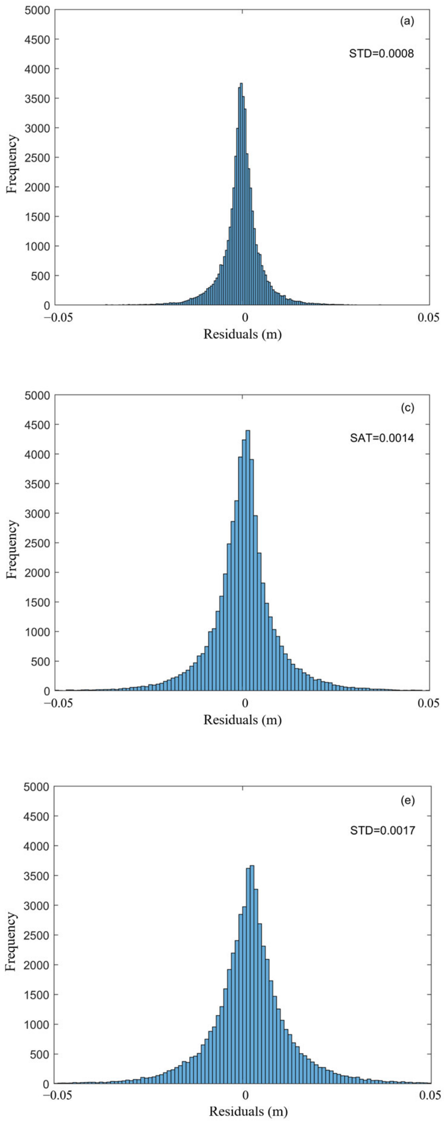

Figure 6. Histograms of the residuals between the InSAR-measured and Weibull-fitted surface uplifts in December 2017 (**a**), December 2018 (**b**), December 2019 (**c**), December 2020 (**d**), and December 2021 (**e**).

4.3. Prediction for Surface Uplift Induced by Groundwater Rebound

The varied Weibull CDF was selected to predict surface uplift induced by groundwater rebound in the Taiji and Guanshan abandoned mines. More specifically, the model parameters of the varied Weibull CDF were estimated using Equation (8) in a least-square sense based on InSAR-measured historical uplifts on a point-to-point basis. The potential future surface uplifts were point-wisely predicted based on the varied Weibull CDF and its inverted parameters. Figure 7 plots the potential surface uplift in the Taiji and Guanshan abandoned coal mines predicted by the varied Weibull CDF in December of 2022, 2023, and 2024, respectively. As is shown in Figure 7, the maximum uplift will increase up to 0.16 m and 0.125 m in the Taiji and Guanshan abandoned coal mines.

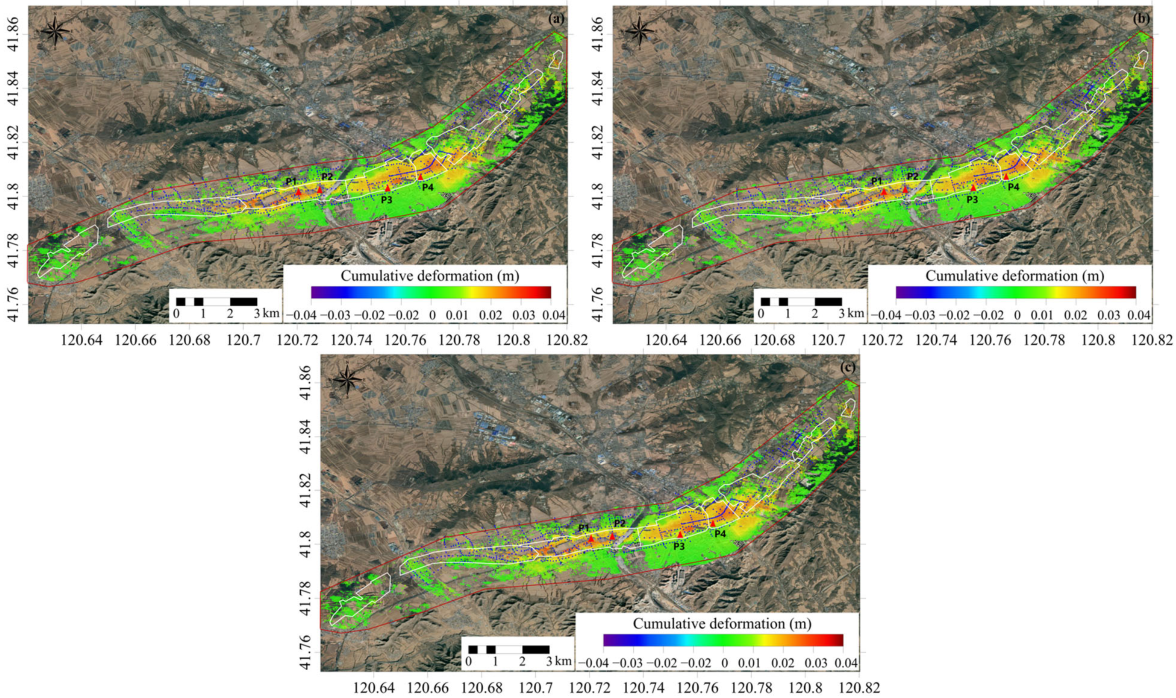

Figure 7. Predicted surface uplifts in the Taiji and Guanshan coal mines in December of (**a**) 2022, (**b**) 2023, and (**c**) 2024, respectively. P1–P4 indicates four surface points with significant uplifts in the period of the collected SAR acquisitions.

In fact, it can be observed from Figures 6 and 7 that, except for the TJ Fourth and GS Third mining regions, the surface uplifts in the remaining mining regions in the Taiji and Guanshan abandoned coal mines has kept approximately stable since the spring of 2019. As the temporal evolution of surface uplifts is linearly proportional to the level changes of groundwater recovery in abandoned mines, we inferred that the groundwater levels in these mining regions have been roughly stable as well since the spring of 2019. Unfortunately, the guess cannot be undoubtably proven due to the lack of in situ observations of groundwater levels in these two abandoned coal mines. As recorded by the official administrator of these two abandoned coal mines, water flowed out of the vertical mine shafts in the GS Second and TJ East mining regions, respectively, in January 2019. This record, to some extent, suggests that the groundwater levels in these two abandoned coal mines approximately remained stable after January 2019.

4.4. Accuracy Evaluation of the Predicted Surface Uplifts

A total of 704 field points were deployed in the Taiji and Guanshan abandoned coal mines in the year of 2021 (their locations are marked by black circles in Figure 7), which were monitored by levelling in October 2021 and April 2022, respectively. These leveling measurements of surface vertical displacements during October 2021 and April 2022 were used to validate the accuracy of the predicted surface uplifts with the varied Weibull CDF in the same period. Figure 8 shows a scatter plot of the leveling-monitored and Weibull-predicted surface uplifts. As is shown in Figure 8, ground surface uplifts in the Taiji and Guanshan abandoned coal mines were roughly stable since October 2021, because leveling observations of vertical displacements in the following six months were mainly within ± 3 mm. In addition, as observed from Figure 8, the surface uplifts predicted by the varied Weibull CDF at the 704 points demonstrated a stable pattern as well, with the uplift magnitudes ranging from 0 to 2 mm. Hence, the predicted uplifts are in good agreement with the leveling observations (serving as reference), with a root mean square error (RMSE) of 1.2 mm. This result suggests that the surface uplifts predicted by the varied Weibull CDF in these two coal mines are reliable.

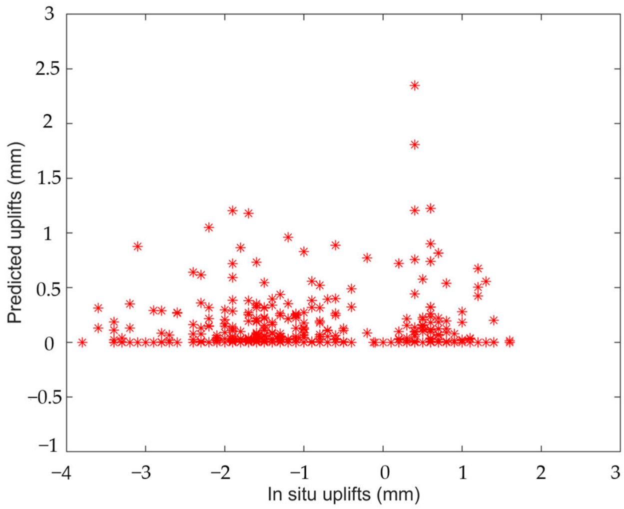

Figure 8. Scatter plot of surface uplifts monitored by leveling (i.e., in situ uplifts) and predicted by the varied Weibull CDF at the 704 field points.

5. Discussions

5.1. Analysis on the Spatial Pattern of Ground Surface Uplifts

As is seen in Figure 3, significant surface uplift occurred in the west and east mining regions of the Taiji abandoned coal mine (denoted by TJ West and TJ East in Figure 3, respectively), whereas surface uplift in the fourth mining region (denoted by TJ Fourth) was insignificant. This phenomenon is highly related to closure history in these three mining regions. More specifically, the fourth mining region was closed in about 2005, and the main phase of surface uplift caused by groundwater rebound was most likely to be completed by April 2017, since the rising curve of groundwater recovery in abandoned mines approximately follows an exponential distribution. The west and east mining regions of the Taiji coal mine were closed in 2014, and parts of the main phase of groundwater rebound-induced surface uplift there were captured by the collected Sentinel-1 SAR images in the period from 2017 to 2021.

A similar spatial pattern of surface uplift can also be observed in the Guanshan abandoned coal mine as well. The third mining region in the Guanshan coal mine (denoted by GS Third in Figure 3) was closed in 2001, and the main phase of surface uplift should have been missed by the collected Sentinel-1 SAR images from 2017 to 2021. However, the first and second mining regions in the Guanshan coal mine (denoted by GS First and GS Second, respectively in Figure 3) were closed in 2014. The surface uplift associated with groundwater rebound could also be detected by the collected Sentienel-1 acquisitions.

Figure 9 plots the kinematic vertical displacements in the Taiji and Guanshan abandoned coal mines along the AA′ profile. Noting this, the missed vertical displacements along the AA′ profile due to low interferometric coherence were interpolated by a Kriging interpolation algorithm, for the sake of visual analyses. As is observed in Figure 9, ground surface along the AA′ profile in the TJ Fourth mining region deformed insignificantly. However, ground surface uplifted exponentially with a cumulative uplift from about 20 mm to a maximum one of around 100 in October 2021, when the AA′ profile went through the TJ West region. When the AA′ profile went from the TJ West to the TJ East regions, the maximum surface uplifts roughly remained stable, although oscillation occurred. Following that, a V-shaped uplift curve was observed, for which the bottom of the V-shaped curve was on the boundary between the Taiji and Guanshan coal mines. Finally, the surface uplifts kept approximately stable with oscillation in the GS Second and GS First mining regions, and then they declined rapidly in the GS Third mining region.

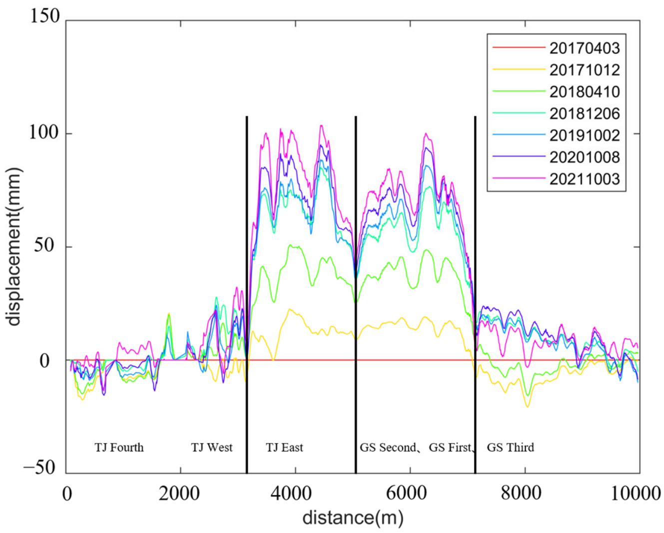

Figure 9. Time-series surface uplifts along the AA′ profile, whose location is marked by a purple dashed line in Figure 3. In which, the legend "20170403" means 3 April 2014.

Such a spatial pattern of surface uplifts along the AA′ profile is possibly due to a hydraulic connection between different mine goafs (referred to ponds). Theoretically, mining coal seams likely results in cracks in overlying rock strata with a wider range than the width of the extracted underground mine goaf [39]. In addition, the goafs in the same coal mining region are generally close to each other or are even connected by tunnels to each other for the maximization of coal production. Consequently, it is possible that cracks in the overlying rock strata due to the extraction of multiple underground mine goafs are connective. In this case, the rising level of groundwater rebound would be nearly the same in the mining region (see the sketch diagram in Figure 10a) due to the influence of hydraulic connection between different ponds [27]. The hydraulic connection is possibly the main reason for the spatial patterns of surface uplift in the TJ West, TJ East, GS First, and GS Second mining regions, respectively.

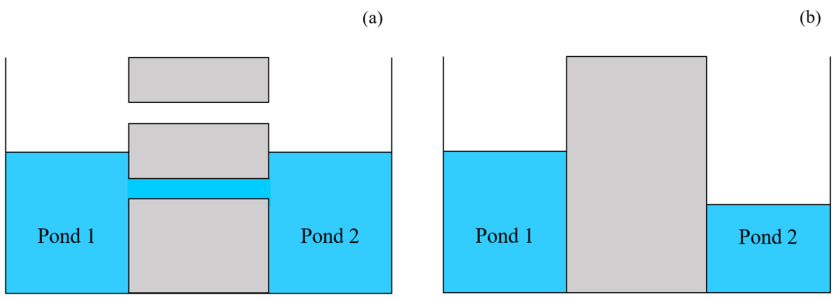

Figure 10. Sketch diagram hydraulic conditions between two connective (**a**) and isolated (**b**) ponds in the abandoned coal mine [27].

However, as is shown in Figure 10b, when mining-induced rock cracks or other water flow courses do not cross rock strata overlying different mine ponds, the ponds are spatially isolated. In this case, the rising level of groundwater rebound of different ponds would be independent, and surface uplift due to groundwater rebound in two isolated ponds would possibly be smaller than that in two connective ponds [27]. Since the Taiji and Guanshan coal mines belonged to two companies, safety pillars were formed on the boundary of these two coal mines. Hence, the ponds in these two abandoned coal mines are theoretically isolated. This is the main reason for the V-shaped uplift curve that occurred along the AA′ profile in the boundary between two focused abandoned mines.

5.2. Modelling Comparison between the Varied Weibull CDF and a Varied Exponential CDF

Theoretically, there are a set of candidate models that can be potentially selected to model the time-series surface uplift induced by groundwater rebound in abandoned mines on a point-by-point basis, in which a varied exponential CDF includes a parameter of the maximum surface uplift (namely d_u^0):

$$d_u(t, P) = d_u^0 \cdot F_{\exp}(t, \lambda) = d_u^0 \left(1 - e^{-\lambda t}\right),\ t \geq 0 \tag{9}$$

which is a typical candidate model, since it is a classical exponential CDF with a variable maximum value. Therefore, we compared the fitting performance between the varied exponential CDF and the varied Weibull CDF used in this study based on the time-series uplifts at the selected points P1–P4. The results are shown in Figure 8, and the corresponding R-squares for the goodness of fit are listed in Table 2 for comparison.

As can be seen from Figure 5, the varied exponential CDF with two parameters is able to roughly describe the temporal processing of time-series surface uplifts by visualization. This conclusion, to a large extent, can be proven by the quantitative indicator of R-squares, whose values range from 0.74 (for point P4) to 0.94 (for point P2), with a mean of 0.74 at these four points. However, Figure 5 also shows that the mis-fitting between InSAR-detected uplifts and the fitted uplifts with the varied exponential CDF (blue lines) is larger than that for the varied Weibull CDF (red lines) used in this study. The mean R-square at these four points for the varied exponential CDF was smaller (0.12) than that for the varied Weibull CDF.

The main reason for the different performance on fitting was due to the parameter numbers in these two models. The varied exponential CDF (i.e., Equation (9)) involved two model parameters (i.e., d_u^0 and λ), whereas the varied Weibull CDF (i.e., Equation (3)) included three model parameters (i.e., d_u^0, η, and β). In fact, the varied exponential CDF is a specific case of the varied Weibull CDF, where $\beta = 1$. Owing to the involved extra parameter of β in the varied Weibull CDF, it is more flexible to model time-series surface uplift and further attribute to a smaller misfitting than the varied exponential CDF.

However, it was noted that adding the extra parameter possibly increased the likelihood to result in overfitting. To test the likelihood, Akaike's information criterion (AIC) was used in this section. AIC is a well-known model selection criterion that penalizes models that use too many parameters to describe the data [40]. Therefore, a model with lower AIC is generally preferred among model candidates, since it can make a better trade-off between model complexity and fitting performance on the given dataset. Table 2 lists the AIC values on the surface uplifts at the points P1–P4 fitted by the varied exponential CDF and the varied Weibull CDF, respectively. As is shown in Table 2, the AIC values for the varied exponential CDF are these four points ranging from 161 to 323 (with a mean of 260), which are about four times the AIC values for the varied Weibull CDF (ranging from 17 to 119, with a mean of 64). This result indicates that, compared to the varied exponential CDF, the varied Weibull CDF is preferred since it takes a better trade-off between model complexity and model fitting performance.

5.3. Influence of InSAR Observations on the Parameter Inversion of the Varied Weibull CDF

Besides the model uncertainties, the accuracy of the predicted surface uplifts in abandoned coal mines using the presented method primarily depends on the reliability of the inverted parameters of the varied Weibull CDF. In this study, the parameters of the varied Weibull CDF were estimated from InSAR observations in an LS sense. Mathematically, the accurate parameter inversion of a nonlinear function usually requires observations covering the key features of the function curve. For instance, Figure 11 shows an uplift curve simulated by the varied Weibull CDF with parameters of $d_u^0 = 100$ mm, $\eta = 0.8$, and $\beta = 2.5$. The main shape of the curve theoretically depends on two uplifts at two special epochs where the maximum uplift velocity and the minimum uplift acceleration occur (namely t_{max_vel} and t_{min_acc}, marked by red circles). This implies that the parameters of the varied Weibull CDF can be uniquely inverted if time-series InSAR observations at these two special epochs are available.

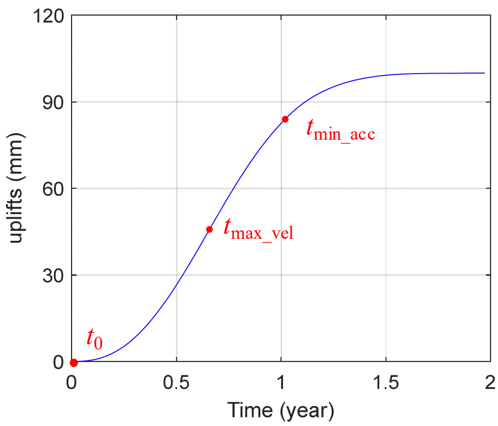

Figure 11. Time-series uplift curve simulated by the varied Weibull CDF under $d_u^0 = 100$ mm, $\eta = 0.8$, and $\beta = 2.5$.

A simulation analysis was conducted to validate the hypothesis. Firstly, we cropped 21 time-series uplifts from t_0 (i.e., the initial date of surface uplifts) to t_{max_vel} from the simulated uplift curve, with a time separation of 12 days (the same as the repeated cycle of a single Sentinel-1 satellite). Gaussian noises with a mean of zero and deviation of 5 mm were then added to the cropped uplifts to simulate time-series InSAR observations. Thirdly, the parameters of the varied Weibull CDF were inverted from the simulated time-series InSAR observations. In order to reduce the randomness of the parameter inversion, we repeated the above inversion procedure 2000 times. For the sake of comparison, time-series InSAR observations from t_0 to t_{min_acc} were simulated with the same procedure and noise levels, and the parameters of the varied Weibull CDF were inverted 2000 times as well.

Figure 12 plots the histograms of the parameters of the varied Weibull CDF inverted with the InSAR observations from t_0 to t_{max_vel} (marked by green) and from t_0 to t_{min_acc}(marked by red), respectively. As is shown in Figure 12, the Gaussian errors caused a significant uncertainty in the inverted parameters, on one hand, when InSAR observations in the period from t_0 to t_{max_vel} were used. The mean standard deviation occurred for 19.8% of the inverted parameters. On the other hand, the same level of Gaussian noise caused a much smaller uncertainty in the inverted parameters (the mean standard deviation occupied 2.2%) when time-series InSAR observations between t_0 and t_{min_acc} were used. This result suggests that InSAR observations spanning a longer period of surface uplifts are beneficial to enhance the robustness of the parameter inversion.

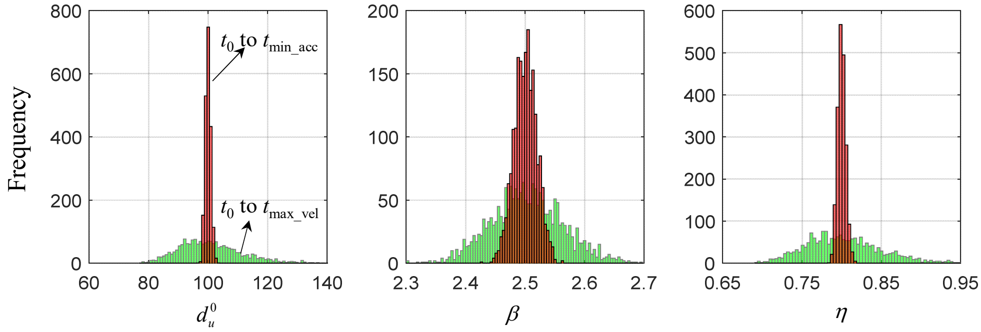

Figure 12. Histograms of the inverted parameters of the varied Weibull CDF with time-series InSAR observations from t_0 to $t_{\text{max\_vel}}$(marked by green) and from t_0 to $t_{\text{min\_acc}}$(marked by red), respectively.

Figure 13 plots the mean and uncertainties of the uplifts predicted by the 2000 sets of inverted parameters using different InSAR observation datasets, in which the red circles represent the error-free InSAR observations. As is seen in Figure 13a, the mean uplifts (green dashed line) agreed well with the simulated ones (blue line), which indicates that the inversion strategy used in this study is able to reliably invert the parameters of the varied Weibull CDF. However, it was observed from Figure 13b that the STDs of the predicted uplifts gradually increased from 0.1 mm to 5 mm (nearly equal to the STD of the added Gaussian noises). When the InSAR observations between t_0 and $t_{\text{min\_acc}}$ were used (see Figure 13b), the STDs of the predicted surface uplifts decreased dramatically (with a maximum STD of 0.9 mm). These results suggest that: (i) the accuracy of the predicted uplifts using the proposed method would decrease with the increase of the predicted periods; (ii) it is beneficial to increase the accuracy of the predicted uplifts using updated InSAR observations.

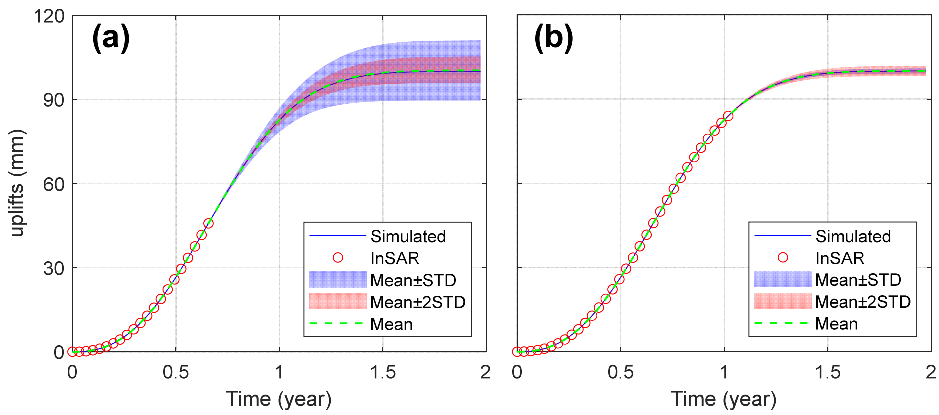

Figure 13. Influences of InSAR time-series observations between t_0 and $t_{\text{max\_vel}}$ (**a**) and between t_0 and $t_{\text{min\_acc}}$ (**b**), respectively, on the predicted uplifts.

6. Conclusions

In this study, the temporal evolution of surface uplifts in abandoned mines was analyzed and further modelled by a varied Weibull CDF on a point-by-point basis. Then, the parameters of the varied Weibull CDF were inverted based on InSAR observations and were used to predict uplift trends. The real data tests in two abandoned mines in Beipiao city, China, suggest that the varied Weibull CDF is able to well describe the processing of surface uplifts caused by groundwater rebound. The comparison between the predicted uplifts and the levelling uplift observations at 704 points showed an RMSE of about 1.19 mm. Compared to the existing InSAR-based numerical analysis methods, in-site geological and hydrological information of the focused abandoned coal mines are not necessary for the presented method. Consequently, the presented method can work well in a wide area without requiring collecting in situ geological and hydrological parameters. However, it should be pointed out that, due to the influence of InSAR observation errors, the accuracy of the predicted uplifts would decrease with an increase of prediction periods. Therefore, in the future, we will attempt to improve the prediction robustness by updating time-series InSAR observations. In addition, we are aware that it is insufficient to validate the feasibility and applicability of the presented method with just two abandoned coal mines in Beipiao city. Therefore, we will test the presented method with more real cases.

Author Contributions: Conceptualization, X.Y. and Z.Y.; methodology, X.Y., J.C. and Z.Y.; software, J.C., and W.D.; validation, G.T. and C.G.; formal analysis, Z.Y.; writing—original draft preparation, X.Y. and J.C.; writing—review and editing, Z.Y.; visualization, J.C., G.T. and C.G.; supervision, Z.Y.; project administration, X.Y. and Z.Y.; funding acquisition, X.Y. and Z.Y. All authors have read and agreed to the published version of the manuscript.

Funding: This research was funded by the National Natural Science Foundation of China, grant number No. 42274057, the Science and Technology Innovation Program of Hunan Province under Grant No. 2021RC3008, the Research Foundation of Education Bureau of Hunan Province, China under Grant No. 20K134, and Central South University Innovation-Driven Research Programme under Grant No. 2023CXQD006.

Data Availability Statement: The used Sentinel-1 data are open access from ESA.

Acknowledgments: We also thank the ESA for providing the Sentinel-1 data (available from the Copernicus Open Access Hub, https://scihub.copernicus.eu/ accessed on 24 September 2022).

Conflicts of Interest: The authors declare no conflict of interest.

References

1. Zhang, H.; Xu, G.; Zhan, H.; Chen, X.; Liu, M.; Wang, M. Identification of hydrogeochemical processes and transport paths of a multi-aquifer system in closed mining regions. *J. Hydrol.* **2020**, *589*, 125344. [CrossRef]
2. Younger, P.L. A simple, low-cost approach to predicting the hydrogeological consequences of coalfield closure as a basis for best practice in long-term management. *Int. J. Coal Geol.* **2016**, *164*, 25–34. [CrossRef]
3. Heitfeld, M.; Mainz, M.; Schetelig, M. Ground heave induced by mine water recovery. In *Eurock 2006: Multiphysics Coupling and Long Term Behaviour in Rock Mechanics*; Taylor & Francis Group: London, UK, 2006; pp. 315–320.
4. Hooper, A.; Zebker, H.; Segall, P.; Kampes, B. A new method for measuring deformation on volcanoes and other natural terrains using InSAR persistent scatterers. *Geophys. Res. Lett.* **2004**, *31*. [CrossRef]
5. Ferretti, A.; Fumagalli, A.; Novali, F.; Prati, C.; Rocca, F.; Rucci, A.J. A new algorithm for processing interferometric data-stacks: SqueeSAR. *IEEE Trans. Geosci. Remote Sens.* **2011**, *49*, 3460–3470. [CrossRef]
6. Berardino, P.; Fornaro, G.; Lanari, R.; Sansosti, E. A new algorithm for surface deformation monitoring based on small baseline differential SAR interferograms. *IEEE Trans. Geosci. Remote Sens.* **2002**, *40*, 2375–2383. [CrossRef]
7. Osmanoğlu, B.; Sunar, F.; Wdowinski, S.; Cabral-Cano, E. Time series analysis of InSAR data: Methods and trends. *ISPRS J. Photogramm. Remote Sens.* **2016**, *115*, 90–102. [CrossRef]
8. Xue, F.; Lv, X.; Dou, F.; Yun, Y. A review of time-series interferometric SAR techniques: A tutorial for surface deformation analysis. *IEEE Geosci. Remote Sens. Mag.* **2020**, *8*, 22–42. [CrossRef]
9. Eriksen, H.Ø.; Lauknes, T.R.; Larsen, Y.; Corner, G.D.; Bergh, S.G.; Dehls, J.; Kierulf, H.P. Visualizing and interpreting surface displacement patterns on unstable slopes using multi-geometry satellite SAR interferometry (2D InSAR). *Remote Sens. Environ. Interdiscip. J.* **2017**, *191*, 297–312. [CrossRef]
10. Ryder, I.; Parsons, B.; Wright, T.J.; Funning, G.J. Post-seismic motion following the 1997 Manyi (Tibet) earthquake: InSAR observations and modelling. *Geophys. J. Int.* **2007**, *169*, 1009–1027. [CrossRef]
11. Henderson, S.T.; Pritchard, M.E. Decadal volcanic deformation in the Central Andes Volcanic Zone revealed by InSAR time series. *Geochem. Geophys. Geosystems* **2013**, *14*, 1358–1374. [CrossRef]
12. Kim, J.; Lin, S.Y.; Singh, R.P.; Lan, C.W.; Yun, H.W. Underground Burning of Jharia Coal Mine (India) and Associated Surface Deformation Using InSAR Data. *Int. J. Appl. Earth Obs. Geoinf.* **2021**, *103*, 102524. [CrossRef]
13. Shi, J.; Yang, Z.; Wu, L.; Niu, J. Large-Gradient Interferometric Phase Unwrapping Over Coal Mining Areas Assisted by a 2-D Elliptical Gaussian Function. *IEEE Geosci. Remote Sens. Lett.* **2022**, *19*, 1–5. [CrossRef]
14. Yang, Z.; Zhu, J.; Xie, J.; Li, Z.; Wu, L.; Ma, Z. Resolving 3-D Mining Displacements From Multi-Track InSAR by Incorporating With a Prior Model: The Dynamic Changes and Adaptive Estimation of the Model Parameters. *IEEE Trans. Geosci. Remote Sens.* **2022**, *60*, 1–10. [CrossRef]
15. Tabish, R.; Yang, Z.; Wu, L.; Xu, Z.; Cao, Z.; Zheng, K.; Zhang, Y. Predicting the Settlement of Mine Waste Dump Using Multi-Source Remote Sensing and a Secondary Consolidation Model. *Front. Environ. Sci.* **2022**, *10*, 526. [CrossRef]

16. Blachowski, J.; Ellefmo, S.L. Mining Ground Deformation Estimation Based on Pre-Processed InSAR Open Data—A Norwegian Case Study. *Minerals* **2023**, *13*, 328. [CrossRef]
17. Yang, Z.; Xu, B.; Li, Z.; Wu, L.; Zhu, J. Prediction of Mining-Induced Kinematic 3-D Displacements From InSAR Using a Weibull Model and a Kalman Filter. *IEEE Trans. Geosci. Remote Sens.* **2022**, *60*, 1–12. [CrossRef]
18. Miao, F.; Zhao, F.; Wu, Y.; Li, L.; Xue, Y.; Meng, J. A novel seepage device and ring-shear test on slip zone soils of landslide in the Three Gorges Reservoir area. *Eng. Geol.* **2022**, *307*, 106779. [CrossRef]
19. Miao, F.; Zhao, F.; Wu, Y.; Li, L.; Török, Á. Landslide susceptibility mapping in Three Gorges Reservoir area based on GIS and boosting decision tree model. *Stoch. Environ. Res. Risk Assess.* **2023**, *2*, 1–21. [CrossRef]
20. Cuenca, M.C.; Hooper, A.J.; Hanssen, R.F. Surface deformation induced by water influx in the abandoned coal mines in Limburg, The Netherlands observed by satellite radar interferometry. *J. Appl. Geophys.* **2013**, *88*, 1–11. [CrossRef]
21. Blachowski, J.; Kopeć, A.; Milczarek, W.; Owczarz, K.J.S. Evolution of secondary deformations captured by satellite radar interferometry: Case study of an abandoned coal basin in SW Poland. *Sustainability* **2019**, *11*, 884. [CrossRef]
22. Cigna, F.; Banks, V.J.; Donald, A.W.; Donohue, S.; Graham, C.; Hughes, D.; McKinley, J.M.; Parker, K.J.G. Mapping ground instability in areas of geotechnical infrastructure using satellite InSAR and Small UAV surveying: A case study in Northern Ireland. *Geosciences* **2017**, *7*, 51. [CrossRef]
23. Gee, D.; Bateson, L.; Grebby, S.; Novellino, A.; Sowter, A.; Wyatt, L.; Marsh, S.; Morgenstern, R.; Athab, A. Modelling groundwater rebound in recently abandoned coalfields using DInSAR. *Remote Sens. Environ.* **2020**, *249*, 112021. [CrossRef]
24. Vervoort, A.; Declercq, P.-Y. Upward surface movement above deep coal mines after closure and flooding of underground workings. *Int. J. Min. Sci. Technol.* **2018**, *28*, 53–59. [CrossRef]
25. Yu, Z.; Huang, G.; Zhang, C. Monitoring and Characterization of Surface Deformation after the Closure of Coal Mines Based on Small Baseline Interferometric Synthetic Aperture Radar. *Instrum. Mes. Métrologie* **2020**, *19*, 141–150. [CrossRef]
26. Gee, D.; Sowter, A.; Athab, A.; Grebby, S.; Wu, Z.; Boiko, K. Remote monitoring of minewater rebound and environmental risk using satellite radar interferometry. *Sci. Total. Environ.* **2023**, *857*, 159272. [CrossRef] [PubMed]
27. Zhao, J.; Konietzky, H. An overview on flooding induced uplift for abandoned coal mines. *Int. J. Rock Mech. Min. Sci.* **2021**, *148*, 104955. [CrossRef]
28. Zhao, J.; Konietzky, H. Numerical analysis and prediction of ground surface movement induced by coal mining and subsequent groundwater flooding. *Int. J. Coal Geol.* **2020**, *229*, 103565. [CrossRef]
29. Adams, R. A Review of Mine Water Rebound Predictions from the VSS–NET Model. *Mine Waterthe Environ.* **2014**, *33*, 384. [CrossRef]
30. Whitworth, K.R. The monitoring and modelling of mine water recovery in UK coalfields. *Geol. Soc. Lond. Spec. Publ.* **2002**, *198*, 61–73. [CrossRef]
31. Younger, P.L.; Adams, R. *Predicting Mine Water Rebound*; Northumbrian Water Ltd.: Durham, UK, 1999.
32. David, G.; Luke, B.; Andrew, S.; Stephen, G.; Alessandro, N.; Francesca, C.; Stuart, M.; Carl, B.; Lee, W. Ground Motion in Areas of Abandoned Mining: Application of the Intermittent SBAS (ISBAS) to the Northumberland and Durham Coalfield, UK. *Geosciences* **2017**, *7*, 85.
33. Chang, L.; Hanssen, R.F. A probabilistic approach for InSAR time-series postprocessing. *IEEE Trans. Geosci. Remote Sens.* **2015**, *54*, 421–430. [CrossRef]
34. Zhu, J.; Li, Z.; Hu, J. Research Progress and Methods of InSAR for Deformation Monitoring. *Acta Geod. Et Cartogr. Sin.* **2017**, *46*, 1717.
35. Fialko, Y.; Simons, M.; Agnew, D. The complete (3-D) surface displacement field in the epicentral area of the 1999 Mw7. 1 Hector Mine earthquake, California, from space geodetic observations. *Geophys. Res. Lett.* **2001**, *28*, 3063–3066. [CrossRef]
36. Li, Z.W.; Yang, Z.F.; Zhu, J.J.; Hu, J.; Wang, Y.J.; Li, P.X.; Chen, G.L. Retrieving three-dimensional displacement fields of mining areas from a single InSAR pair. *J. Geod.* **2015**, *89*, 17–32. [CrossRef]
37. Sica, F.; Cozzolino, D.; Zhu, X.X.; Verdoliva, L.; Poggi, G. InSAR-BM3D: A nonlocal filter for SAR interferometric phase restoration. *IEEE Trans. Geosci. Remote Sens.* **2018**, *56*, 3456–3467. [CrossRef]
38. Chen, C.W.; Zebker, H.A. Two-dimensional phase unwrapping with use of statistical models for cost functions in nonlinear optimization. *J. Opt. Soc. Am. A* **2001**, *18*, 338–351. [CrossRef]
39. Kratzsch, H. *Mining Subsidence Engineering*; Springer Science & Business Media: Berlin/Heidelberg, Germany, 2012.
40. Chakrabarti, A.; Ghosh, J.K. AIC, BIC and recent advances in model selection. *Philos. Stat.* **2011**, *7*, 583–605.